Heliyon 6 (2020) e02803

Contents lists available at ScienceDirect

Heliyon

journal homepage: www.heliyon.com

Heliyon

Research article

A hydro-thermal-geochemical modeling framework to simulate reactive transport in a waste coal area under amended and non-amended conditions

Yi Xu [a], Fernando J. Plaza [a], Xu Liang [a,*], Tyler W. Davis [a,b], Judodine Nichols [c], Jaw K. Fu [c], Peter Koranchie-Boah [c]

[a] Department of Civil and Environmental Engineering, University of Pittsburgh, Pittsburgh, PA, USA
[b] Center for Geospatial Analysis, William & Mary, Williamsburg, VA, USA
[c] Alcoa Technical Center, New Kensington, PA, USA

ARTICLE INFO

Keywords:
Environmental science
Ecology
Environmental geochemistry
Environmental hazard
Environmental pollution
Hydrology
Coal refuse
Acid mine drainage
Bauxite residue
Environmental impacts
Hydro-thermal-geochemical model
Pyrite oxidation

ABSTRACT

Acid mine drainage (AMD) is a major cause of water quality deterioration across watersheds where acidic coal refuse (CR) piles are located. The oxidation of pyrite (the most common sulfide mineral), found in many of the CR piles, releases major ions, such as Fe^{2+}, Fe^{3+}, SO_4^{2-}, and H^+ into the environment. Bauxite residue (BR), commonly called alkaline clay (AC), a highly alkaline byproduct of the alumina refining process, can be combined with coal mine refuse to reduce and potentially eliminate the AMD problem associated with waste coal piles. A new hydro-thermal-geochemical model is developed in this study to simulate the reactive transport processes in AMD-treated areas. First, the model is tested at the experimental plots located within a CR pile in Greene County, Pennsylvania (USA), where two of the plots are used to show the impact of BR on CR piles. Then, the model capabilities are tested at a mine-impacted watershed in Indiana County, Pennsylvania (USA). In general, the model not only captures the patterns of both soil moisture, soil temperature and chemical concentrations at plots scales but it is also successfully implemented at a watershed scale. In conclusion, this study shows encouraging results regarding the AMD remediation simulation at different spatial scales.

1. Introduction

Small mountains of overburden and low-energy-value materials have been left behind from long-term industrial developments. They are commonly known as coal refuse (CR) or "gob" piles. These deposits, which typically have a deep unsaturated soil layer, also have a highly heterogeneous mineral composition with the potential of releasing acidity, metals and other harmful elements into the environment. The majority of these hydro-geochemical processes occurs due to the oxidation of sulfide minerals (e.g., pyrite) that contribute to acid mine drainage (AMD) (Johnson and Hallberg, 2005), a major environmental issue in natural waterways due to the considerable amount of coal-powered energy produced globally. A new approach to treat AMD is investigated in this study: to combine bauxite residue (BR), a highly-alkaline byproduct of the alumina refining process, with coal refuse (CR), which has high acidity potential. To facilitate the investigation of impacts of this new approach, a new model, which takes into account both the hydrological and pyrite oxidation processes (and their interactions), is developed.

Currently, a few models exist that can simulate the hydrological and geochemical processes for AMD studies. In general, these models are based on the HYDRUS (Šimůnek et al., 1998, 1999) or TOUGH2 model frameworks, or the mass conservation equation governing the flow of multiphase fluids (Pruess, 1991), or simply a direct use of the Richards' Equations to describe water movement in the soil porous media.

HYDRUS utilizes the advection-dispersion equation and incorporates a sequential first-order decay formula to mimic the behavior of chemicals in soil water. It is a multi-phase model that is typically applied to a one-dimensional soil profile (e.g., HYDRUS-1D (Šimůnek et al., 1998)) or a two-dimensional field (e.g., HYDRUS-2D (Šimůnek et al., 1999)). Geochemical features have been considered in HYDRUS by coupling with geochemical model. For example, HP1 (Jacques et al., 2006; Šimůnek et al., 2008) is a 1D hydro-geochemical model which couples HYDRUS-1D with PHREEQC v2.0 (Parkhurst and Appelo, 1999). POLYMIN (Molson et al., 2005) was developed based on HYDRUS-2D. It includes the features of the shrinking core model (Davis and Ritchie, 1986)

* Corresponding author.
E-mail address: xuliang@pitt.edu (X. Liang).

https://doi.org/10.1016/j.heliyon.2019.e02803
Received 2 August 2019; Received in revised form 13 September 2019; Accepted 31 October 2019

and the features of MINTEQA2 (Allison et al., 1991), which is able to simulate hydro-geochemical processes in the profile of a CR pile. Another AMD model, THERMOX (Silva, 2004), combines HYDRUS-2D with the early version of a pH-redox-equilibrium-equations speciation model (i.e., PHREEQC) (Parkhurst et al., 1980) to simulate acid mine drainage in waste rock areas. Furthermore, in 2009, the speciation module in PHREEQC (Parkhurst, 1995) and the shrinking core model were coupled to THERMOX (da Silva et al., 2009) to achieve a more physically-based description of the pyrite oxidation and hydrological processes.

TOUGH AMD (Lefebvre, 1994) is a model that combines TOUGH2 with the concept of the shrinking core model to simulate the process of pyrite oxidation at cross-profile scale on a site. It is similar to MIN3P (Mayer et al., 2002), which also includes the shrinking core model and uses the Richards' Equation to simulate variably-saturated flow. SULFIDOX (Brown et al., 2001) is another model that employs Richards' Equation; however, instead of using the shrinking core model for pyrite oxidation, it considers gas transport as described in its original framework, FIDHELM (Pantelis et al., 2002).

Regarding the geochemical modeling aspects, due to a large number of processes (e.g.: physical, chemical and even biological) occurring in parallel in AMD regions, it is difficult to simulate all these processes with a single model. Since pyrite oxidation is the main contributor to water acidification (Johnson, 2003), it is often considered as a key reaction to be modeled. The shrinking core model is one of the most popular modules to dynamically simulate the pyrite oxidation process in the AMD models. It is usually combined with an oxygen diffusion module to control the oxygen conditions for pyrite oxidation. Wunderly et al. (1996) developed a physically-based model called PYROX that simulates one-dimensional, kinetically-controlled oxygen diffusion within the vadose zone of mine tailings. This model is based on a combination of the oxygen diffusion and shrinking-core modules with a simple reactive transport model. Gerke et al. (1998) used a similar concept for simulating pyrite oxidation on overburden mine spoils. In this approach, the pyrite oxidation process is coupled with a two-dimensional advection-dispersion transport model on a 2D cross-sectional domain. This work has been coupled with HYDRUS-2D to create POLYMIN, and is designed for field-scale applications, such as modeling unsaturated waste rock piles (Molson et al., 2005).

Since the geochemical processes in AMD regions are not only affected by pyrite oxidation but also by other reactions in the waste rock area, geochemical models such as MINTEQA2 (Allison et al., 1991) and PHREEQC, are good candidates for modeling reactions so that the various geochemical characteristics of the coal refuse piles can be taken into account. MINTEQA2 is a geochemical equilibrium speciation model for dissolved, absorbed, solid and gas phases. It includes a large database of thermodynamic data to solve a broad range of problems. It is an adequate model to address the equilibrium environment; however, it does not solve kinetic reactions such as pyrite oxidation. PHREEQC is a one dimensional model, which has been widely used in the geochemical field and was designed with a graphical user interface (Charlton et al., 1997). It calculates the rate of pyrite oxidation by utilizing a derived function based on detailed measurements (Williamson and Rimstidt, 1994). PHREEQC includes a larger dataset based on a wide number of reactions. The range of ionic strength in PHREEQC is larger than MINTEQA2, due to the incorporation of the Pitzer aqueous model in its latest version (Parkhurst and Appelo, 2013).

To date, there is not a suitable physically-based hydro-thermal-geochemical model built upon a distributed hydrology-soil-vegetation-watershed framework, where the water and energy budgets and their interactions are adequately represented, in connection with the pyrite oxidation and other related chemical processes. Some hydrological models include pollutant fate-and-transport processes, but they do not represent the pyrite oxidation process, while others are only designed for site scale (e.g., profile of field cross-section) with simplified calculations on hydrology-soil-vegetation interactions. Although there are models utilizing 2D Richards' equations (e.g., HYDRUS-2D, TOUGH2) in conjunction with the shrinking core model, MINTEQA2, and/or PHREEQC as reviewed above, these models (e.g., POLYMIN) do not fully consider the interactions between water and energy fluxes and their impacts on the pyrite oxidation processes.

To fill in this gap, we are developing a new hydro-thermal-geochemical model (HTGCM) that is adequate to represent water and energy budget including pyrite oxidation and related chemical processes. This new model will be evaluated at an AMD site with available observations to illustrate the model's capability for applications at different spatial scales (e.g., plot and watershed) where interactions among water, temperature and chemical concentrations are accounted for.

2. Methodology

2.1. Model development

2.1.1. Hydrologic cycle

In this study, the Distributed Hydrology Soil Vegetation Model (DHSVM) (Wigmosta et al., 1994) is employed to describe the dynamic movement of water and chemical species associated with two discrete zones, amended and non-amended zones, along the vertical direction. DHSVM also partially considers the effects of horizontal movements of water through its surface and subsurface flow routing processes which are a part of the DHSVM (Wigmosta and Lettenmaier, 1999) to link the horizontal movement of the water and chemical species in this study. Such a 1.5 dimensional (1.5D) approach (i.e., 1D vertical + horizontal routing), instead of 2D or 3D approach, is adequate for the applications at the watershed scale and for areas with deeper unsaturated zone where the vertical flow is typically a dominated one like in this application study, although a 2D or 3D approach would be more appropriate for certain situations if the data availability and computation cost are not a concern. In our 1.5D approach, the vertical flow is calculated for time step t followed by the horizontal routing calculation for that same time step t, and so forth. The model does not calculate the vertical flows for the entire simulation period and then does the routing. In other words, the vertical and horizontal mass balances are not simulated as two completely separated processes in our 1.5D approach, but as two processes that interact with each other at every time step.

Although DHSVM is a well-known distributed hydrologic model that has been widely applied to study problems related to mountainous watersheds with sub-daily timescales (Doten et al., 2006; Leung et al., 1996; Leung and Wigmosta, 1999; Westrick et al., 2002; Whitaker et al., 2002), it needs to be modified for applications to coal mining studies. For instance, CR piles are typically hilly and have steep slopes with large pile depths and complex soil characteristics. To address such unique characteristics, three improvements are made to the DHSVM model.

The first improvement is to add two additional soil layers into the original four-layer soil column as shown in Fig. 1. One of the layers is a buffer layer (i.e., Layer 2) that is comprised of both an amended zone (top half) and a non-amended zone (bottom half). The other layer is a thick bottom layer to mimic the large depth of the CR piles, which can be more than 10-meter deep. The depths of the five top layers (beginning from the surface) are as follows: 0.2 m (layer 0), 0.2 m (layer 1), 0.42 m (layer 2), 1.5 m (layer 3), 4.0 m (layer 4), and around 8.0 m (layer 5). This layer arrangement allows the model to simulate amended and un-amended regions at the same time.

The second improvement is the incorporation of steep slope into infiltration process. As shown by Philip (1991) and Chen and Young (2006), the impact of slope on infiltration becomes significant when the slope is greater than 30°. Along the steep slopes of CR piles, less water infiltrates into the soil column, which translates into more water becoming surface runoff. To account for this, a simple expression (i.e., multiplying the rainfall by the cosine of the slope angle) has been incorporated into DHSVM.

The third improvement is related to its lower boundary condition. Originally, DHSVM assumes a zero-flux boundary condition at the

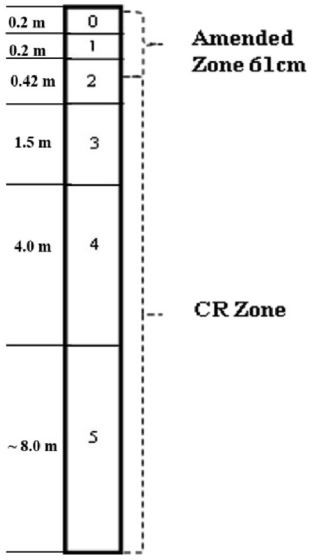

Fig. 1. Layout of soil layer profile in the coal refuse region. The interface between amended and non-amended zone locates at the middle depth of Layer 2 (i.e. 61 cm). Above 61 cm, it is the amended zone, while it is coal refuse below 61 cm.

bottom layer. To allow moisture to exit from the bottom of CR pile and to enter the underlying ground soil, a lower boundary of free drainage condition has been adopted. That is, at the lower boundary the drainage is assumed to be equal to the hydraulic conductivity of the lowest soil layer of the study domain. This assumption is typically valid when the groundwater table is deep (Šimůnek et al., 1998) as in our case.

2.1.2. Geochemical development

HTGCM utilizes the methods of both PYROX and PHREEQC models to represent the geochemically-based pyrite oxidation process, while the advection-dispersion equation (ADE) plays an important role communicating geochemical and hydrological processes. This equation can be expressed as follows:

$$\frac{\partial \theta C}{\partial t}+\frac{\partial \rho k C}{\partial t}=\frac{\partial}{\partial z}\left(\theta D^{w}\frac{\partial C}{\partial z}\right)-\frac{\partial qC}{\partial z}-SS \tag{1}$$

where θ is the volumetric soil moisture content [L^3L^{-3}]; z is soil depth [L], t is time [T], ρ is the soil bulk density [ML^{-3}]; C is the chemical concentrations in the liquid phase [ML^{-3}]; k is an absorption/desorption coefficient; C represents chemical concentrations in solid phase [MM^{-1}]; q is the water flow in soil [LT^{-1}]; D^w is the dispersion coefficient in water [L^2T^{-1}]; and SS is the source/sink term [$MT^{-1}L^{-3}$]. In this study, SS represents the liquid phase of total S, total Fe and other chemicals (e.g., H, Al, Ca, K, Si, Mn, Zn and Ni). This equation is solved by the finite difference method.

The pyrite oxidation process is simplified into two reactions represented below by equations (R1) and (R2) (Kameia and Ohmoto, 2000). These two reactions can also be combined into a single expression shown in equation (R3).

(R1) $FeS_2 + H_2O + 7/2O_2 \Rightarrow Fe^{2+} + 2SO_4^{2-} + 2H^+$

(R2) $Fe^{2+} + 1/4O_2 + H^+ \Rightarrow Fe^{3+} + 1/2H_2O$

(R3) $FeS_2 + 1/2H_2O + 15/4O_2 \Rightarrow Fe^{3+} + 2SO_4^{2-} + H^+$

Applying the algorithm of PYROX developed by Wunderly et al. (1996), the pyrite oxidation process can be represented with two sub-modules: an oxygen diffusion sub-module and a shrinking-core sub-module (Davis and Ritchie, 1986). Under saturated soil conditions, oxygen diffusion is considerably slower than that in the air, thus limiting the pyrite oxidation process (Gerke et al., 1998). In this model, pyrite oxidation is assumed to occur only within the unsaturated soil layers of the coal refuse pile.

The oxygen diffusion and dispersion in the pore space is described by Eq. (2):

$$\frac{\partial \theta_a(z)\cdot[O_2]_a}{\partial t}=\frac{\partial}{\partial z}\left(\theta_a\cdot D_a(z)\cdot\frac{\partial [O_2]_a}{\partial z}\right)-S_{O_2}(z,t) \tag{2}$$

where $\theta_a(z)$ is the air content [L^3L^{-3}], $D_a(z)$ is the oxygen diffusion coefficient in the pore space [L^2T^{-1}], $[O_2]_a$ is the concentration of oxygen in the pore space [ML^{-3}], S_{O_2} is the oxygen consumption treated as a sink term [$ML^{-3}T^{-1}$]. $D_a(z)$ is calculated based on the method of Elberling et al. (1993) and Gerke et al. (1998).

The shrinking-core sub-module assumes that the mineral particles are spherically shaped and homogeneously distributed throughout the coal refuse pile (Gerke et al., 1998; Wunderly et al., 1996). Combining the 1D oxygen transport module with the shrinking-core module, we obtain Eq. (3):

$$\frac{\partial \theta_a\cdot[O_2]_a}{\partial t}=\frac{\partial}{\partial z}\left(\theta_a D_a\frac{\partial [O_2]_a}{\partial z}\right)-D_w^{O_2}\frac{3(1-\theta_s)}{R^2}\left(\frac{r_c}{R-r_c}\right)\frac{[O_2]_a}{H} \tag{3}$$

where the average radius of soil particles is represented as R and the radius of the unreacted mineral cores is r_c, R is set to 2.0 mm and the initial r_c for each layer is 1.95 mm, which are within the range of laboratory experiments; $D_w^{O_2}$ is the effective oxygen diffusion coefficient containing diffusion properties of the water and oxidized mineral particle, which is equal to 3.2×10^{-11} m^2/s (Gerke et al., 1998); θ_s is porosity [L^3L^{-3}]; H is Henry's constant, which is equal to 2.63. The upper boundary of oxygen concentration in the air is set to be a constant of 0.31 kg/m^3, which is obtained based on a standard air condition. The formula of changes of the unreacted mineral core radius (dr_c/dt) has been documented (Gerke et al., 1998). Combining it with Eq. (3), the unreacted particle radius (r_c) and the oxygen concentration $[O_2]_a$ for each soil layer can be solved through the scheme of Wunderly et al. (1996). Then, SO_4 (total sulfate in all SO_4^{2-} chemicals) and Fe (total iron, i.e., Fe(II) plus Fe(III)) from the pyrite oxidation can be estimated. The production of sulfur in the liquid phase is given by:

$$\Delta C_{S,liquid}^{oxid}=\frac{\rho_s|_m\left[\left(r_c|_m^n\right)^3-\left(r_c|_m^{n-1}\right)^3\right]}{\left(R|_m\right)^3\theta|_m} \tag{4}$$

where $\Delta C_{S,liquid}^{oxid}$ is the sulfur produced by pyrite oxidation in the liquid phase at each time step [ML^{-3}]; $\rho_s|_m$ is the sulfur bulk density within the m^{th} layer [ML^{-3}]; $\theta|_m$ is the soil moisture within the m^{th} layer [LL^{-1}]; $r_c|_m^n$ is the unreactive core within the m^{th} layer at the n^{th} time step; and $r_c|_m^{n-1}$ is the unreactive core within the m^{th} layer at the $(n-1)^{th}$ time step. The production of Fe (total) in the liquid phase can thus be derived as:

$$\Delta C_{Fe,liquid}^{oxid}=\frac{W_{Fe}\cdot\Delta C_{S,liquid}^{oxid}}{2.0\times W_s} \tag{5}$$

where W_{Fe} and Ws are the molar mass for iron and sulfur, respectively. The productions from pyrite oxidation play important roles as the source term in Eq. (1). Simultaneously, the other mineral reactions are also taken into account in PHREEQC, which is built into HTGCM.

IPHREEQC (Charlton and Parkhurst, 2011) provides a convenient way to couple PHREEQC's modules with other models by linking the static IPHREEQC library and reaction database of PHREEQC to the targeted model (here it is HTGCM) instead of coupling all of the two models' codes together. This approach reduces the chance of errors and improves the efficiency of model couplings.

The interaction of chemical species among the grid cells is realized through the routing process. The concentrations in adjacent grid cells can

be expressed by the mass balance equation as follows:

$$C_{in,i,j}Q_{in,i,j} = \sum_{k=0}^{7} F_k C_{out,k} Q_{out,k} \tag{6}$$

where $C_{in,i,j}$ and $Q_{in,i,j}$ are the chemical concentrations and inflow at cell (i, j), respectively; F_k is the fraction of the outflow in each direction (Wigmosta and Lettenmaier, 1999); $C_{out,k}$ and $Q_{out,k}$ represent the chemical concentrations and the outflow at the k^{th} direction, respectively.

2.1.3. Heat transport

The heat transport is based on the Fourier's Law, i.e., Eq. (7) and energy conservation equation, i.e., Eq. (8):

$$q_h = -k_h \frac{\partial T}{\partial z} \tag{7}$$

$$Cap_s \frac{\partial T}{\partial t} = \frac{\partial}{\partial z}(-q_h) + \rho_i L_f \left(\frac{\partial \theta}{\partial t}\right) - S_h \tag{8}$$

where q_h is the heat flux [MT^{-3}], k_h represents the soil thermal conductivity [$MLT^{-3}K^{-1}$], Cap_s represents the soil volumetric heat capacity [$ML^{-1}T^{-2}K^{-1}$], T denotes the soil temperature [K], ρ_i denotes the density of ice [ML^{-3}], L_f is the latent heat of fusion [L^2T^{-2}] and S_h is a sink/source term. Inserting Eq. (7) into Eq. (8) and using $H_{chemical}$ [$ML^{-1}T^{-3}$] and $H_{biological}$ [$ML^{-1}T^{-3}$] to represent chemical heat and biological heat, respectively, we obtain:

$$Cap_s \frac{\partial T}{\partial t} = \frac{\partial}{\partial z}\left(k_h \frac{\partial T}{\partial z}\right) + \rho_i L_f \left(\frac{\partial \theta}{\partial t}\right) + \left(H_{chemical} + H_{biological}\right) \tag{9}$$

Following the method of Hollesen et al. (2011), the chemical-associated heat from the pyrite oxidation is expressed as:

$$H_{chemical} = heatpro\_A \times e^{(heatpro\_B \times T)} \tag{10}$$

where *heatpro_A* and *heatpro_B* are heat coefficients for chemical reactions. The O'Neill function (Stange, 2007) is used to calculate the biological-associated heat as follows:

$$H_{Biological} = heatpro\_A_2 \cdot \left(\left(\frac{T_{\max} - T}{T_{\max} - T_{opt}}\right)^n \times e^{n \times \left((T - T_{opt})/(T_{\max} - T_{opt})\right)}\right) \tag{11}$$

where T_{opt} [K] is the optimum temperature when the rate of biological oxidation reaches maximum value. T_{max} [K] is the maximum temperature when biological activity ceases, $heatpro\_A_2$ is the rate of heat production and n is the parameter of the O'Neill function. The parameters are set as: n is 10.73, T_{max} = 55 °C and T_{opt} = 25.23 °C (Stange, 2007). Considering the decay pattern of pyrite oxidation, both chemical and biological heat decreases as an exponential function (Hollesen et al., 2011) as follows:

$$H_{chem/bio-current} = H_{chem/bio-begin} \cdot \exp\left(-decay_{chem\_or\_bio} \times number\_of\_timesteps\right) \tag{12}$$

where $decay_{chem\_or\_bio}$ is the half-life period of chemical or biological activities, $H_{chem/bio\_current}$ is the heat production at the current time step, and $H_{chem/bio\_current\_begin}$ is the heat production at the beginning time step.

In this study, the heat sources come from solar radiation, chemical reactions and biological activities. The rates of chemical reactions and transport coefficients are all temperature-dependent. For example, the equilibrium rate between Fe(II) and Fe(III), which is an important factor affecting the rate of pyrite oxidation, depends on the temperature. A general Arrhenius equation (Stumm and Morgan, 1981) that represents the relationship between the temperature and coefficients is used in HTGCM as follows:

$$C_T = C_r \exp\left(\frac{E_a\left(T^A - T_r^A\right)}{R_u T^A T_r^A}\right) \tag{13}$$

where C_T and C_r are the coefficients/rates at an absolute temperature T^A and its reference temperatureT_r^A, respectively; E_a [$ML^2T^{-2}M^{-1}$] is the activation energy of the particular reaction and R_u is the universal gas constant. The reference temperature is assumed to be 25°C in this study. The activation energy, which is not sensitive, is assumed to be 46.0 KJ mol^{-1} for all of the processes.

The above heat module is adequate to serve the goal of simulating the thermal transport in a single cell or within a watershed. Similarly to most of the land surface models, e.g., CLM5.0 (Lawrence et al., 2019), VIC (Liang et al., 1994) and Noah (Mitchell, 2001) as well as some reactive transport models, e.g., POLYMIN and MINTRAN (Walter et al., 1994), HTGCM does not consider the lateral transport for heat. Apparently, this needs to be improved, especially when applied to fine-resolution scales.

2.1.4. Coupling framework in HTGCM

To combine all of the above components together in the HTGCM model, the DHSVM model (i.e., the basic framework) plays an important role in connecting the hydrologic components with the geochemical components and the thermal transport, as shown in Fig. 2. We use sequential coupled approach. The main procedures are: (1) air content is passed from the DHSVM model to PYROX, and chemical concentrations are calculated and communicate between PYROX and PHREEQC; (2) simultaneously, soil water is transferred from the DHSVM model to ADE; (3) soil temperature is passed between thermal transport module and PHREEQC; (4) finally, soil water and chemical concentrations are transported by the routing module and are distributed to the other grid cells. In this study, thermal transportation is assumed to occur only within the vertical direction, while the horizontal distribution will be considered in the future research.

2.2. Study sites and data

We evaluate the newly developed model at two study sites with very different spatial scales: a plot scale (Mather site) and a watershed scale (Ernest coal waste pile site).

2.2.1. Mather site

The Mather coal refuse pile, a remnant of the Pickand-Mather Collieries Mine, was in operation from 1918 to 1964. It is situated along the south branch of Ten Mile Creek in Mather, Greene County, Pennsylvania, USA. Previous reclamation work has reshaped a considerable portion of the coal refuse pile, which now has a vegetated tier and a large plateau (Fig. 3a).

Investigation of the beneficial use of BR in neutralizing the acidic environment and enhancing the soil quality began in 2009 with a two-acre pilot region prepared along the northern face of the Mather coal pile (Fig. 3b). This region was divided into four half-acre plots, three of which were reclaimed according to the reclamation methods listed by the Pennsylvania Department of Environmental Protection (PADEP) and one left non-amended (i.e., plot 1) as a control plot for comparison. Each one of the three reclaimed plots have amended layers, approximately 61 cm deep for plots 2 and 4 and about 91 cm deep for plot 3. AMD was remediated using of 10% bauxite residue (plot 2), 10% bauxite residue + 5% compost (plot 3), and 30% limestone (plot 4). All plots, except plot 1, were hydro-seeded and mulched. The seed mixture consisted of seven types of plant species. Fig. 3c and d depict the before and after conditions of the four plots. All three of the amended plots underwent vegetative growth. In the plot-scale study, the simulations were conducted within the red-dash rectangular area in Fig. 3b where the two-acre pilot region is located and the presented field measurements were from plot 1 and plot 2, since we mainly focused on the differences between the non-amended (i.e., CR) and amended (i.e., CR + BR) scenarios.

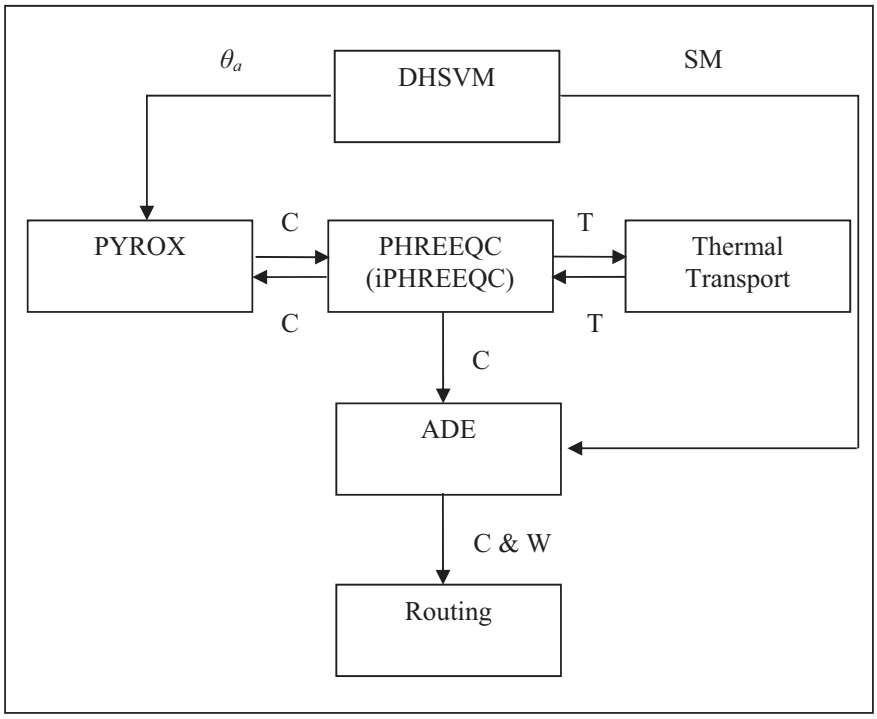

Fig. 2. Flowchart of coupling DHSVM, PYROX, PHREEQC, thermal transport, ADE and routing in HTGCM. Note: C: concentrations, SM: soil moisture, T: temperature, θ_a: air content, W: water.

According to the laboratory measurements, the saturated hydraulic conductivity (Ks) of CR is within a magnitude of 10^{-5}–10^{-4} m/s. Due to the large value of Ks and considerable depth (greater than 10 m), the CR pile has been in an unsaturated state for a long time period. Table 1 illustrates the measurements of the surface porosity and Ks within plot 1, plot 2 and normal soil.

Meteorological data required by the model (e.g., rainfall, air temperature, relative humidity and wind speed) were obtained starting at June 2009 from a local weather station (KPACLARK3), part of the Weather Underground personal weather station online network (https://www.wunderground.com/weatherstation/overview.asp), which is located within a two-mile radius of the study area. Solar radiation data were obtained from the National Solar Radiation Data Base (https://nsrdb.nrel.gov). The forcing data were gathered for the simulation of soil moisture and chemical concentrations. High resolution, 3 × 3 m, DEM (digital elevation model) data were downloaded from the US Geological Survey (USGS) website (https://usgs.gov) to capture the complexity of the topography of the coal refuse pile as much as possible.

Soil moisture and soil temperature sensors (EC-5 and 5TM by Decagon Devices, Inc.) were installed at the middle locations (Fig. 3b) along the hillslope for the plots with the detection limits of $\pm 0.03\ m^3/m^3$ and $\pm 1\ ^\circ C$, respectively. At each location, soil moisture and soil temperature were measured at the depth of 61 cm (i.e., the depth of the interface of the amended and non-amended zones). The retrieval of soil moisture and soil temperature data occurred from May 2012 to October 2012, while the chemical concentration data were collected from June 2009 to June 2010. Lysimeters were proximally installed at the same middle locations along the hillslope in each plot to collect chemical samples. Soil moisture and soil temperature sensors were permanently damaged at plot 1 due to the highly acidic environment; therefore, only measurements of chemical concentrations are available at plot 1.

2.2.2. Ernest coal pile watershed

The Ernest Mine operation is located in White and Rayne Townships, Indiana County, Pennsylvania, USA (Fig. 3e). The operation is utilizing waste coal ash for alkaline addition to treat AMD. The refuse material is taken out, transported to the Cambria CoGeneration power plant, and FBC (i.e., fluidized bed combustion) coal ash produced from burning the refuse is returned and placed on the site. Ash placement commenced in October 1996 and has continued to present. However, results have shown the coal ash addition has not significantly improved the water quality at the mine discharge (Pennsylvania Minefill Study, 2007). This mine has been continuously monitored for over a decade. Moreover, the majority of the sampling sites are located at the mine's drainage discharge, which makes it possible to implement the proposed model in this watershed.

The Ernest watershed shares some similarities with the Mather site: both are coal refuse piles, with similar geographic locations (i.e., Western Pennsylvania, in the Northern Appalachian Coalfield) and they are fairly well characterized. The Ernest site has about two years of data for non-amended conditions and about 8 years of data for amended conditions (i.e., addition of FBC ash).

The entire Ernest watershed includes the mine site, the non-mine region and the location of MW-1 sampling site. The watershed outlet has an important drainage contribution from both inside and outside the mine region. The sampling site (MW-1, which stands for mine well 1) that was used for the model evaluation is located at the watershed outlet. In MW-1, the drainage water is collected at approximately 1.5 meters deep. The parameters that were measured at this sampling site are pH, SO4, Fe, Al, Mn, Ca, Ni and Zn. The required meteorological data were retrieved from a local weather station (KPAINDIA4), which is part of the Weather Underground personal weather station online network, located within a three-mile radius of the study area. Solar radiation data were obtained from the NOAA National Solar Radiation Data Base. The spatial resolution of the DEM data, downloaded from the USGS website, is at the 10 × 10 m resolution.

2.2.3. Model geochemcal input data

The model needs to be initialized with geochemical data: pH, sulfate and metals/nonmetals concentrations (aqueous phase), mineral composition, oxygen concentration, etc. In order to obtain adequate results from the simulations, these data must be based on actual measurements and/or realistic assumptions. For this purpose, the Mather site served as the

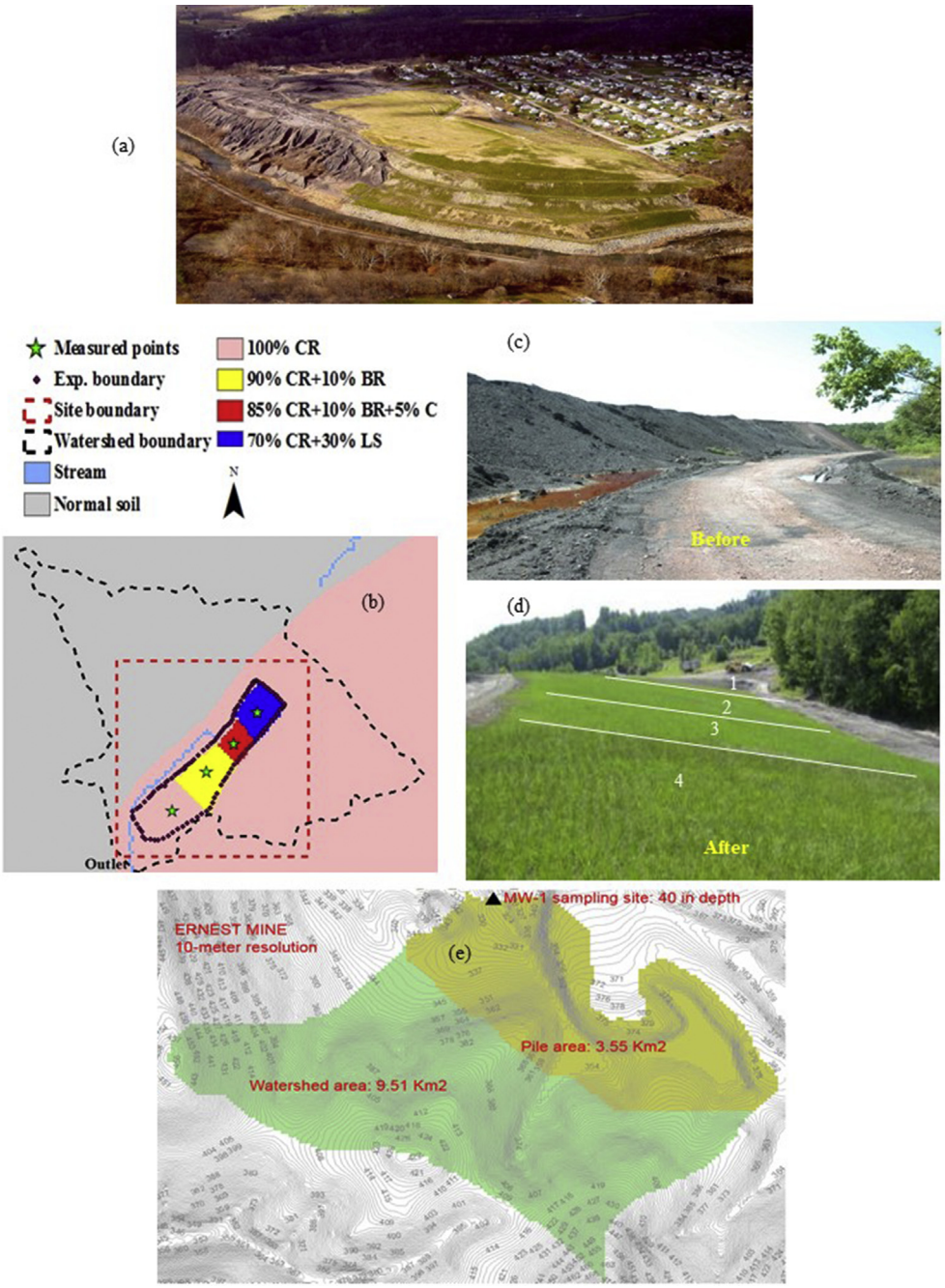

Fig. 3. (a) Coal refuse piles at Mather, Greene County, Pennsylvania. (b) Locations of compared points on the four plots: the green stars are the middle locations along the hill slope where soil sensors and lysimeters are installed. Plot 1 (pink) is the coal refuse without vegetation, plot 2 (yellow) is 90% coal refuse mixed with 10% bauxite residue in the amended zone with vegetation grown on the top, plot 3 (red) is 85% coal refuse mixed with 10% coal refuse and 5% mushroom compost with vegetation grown on the top, and plot 4 (blue) is 70% coal refuse mixed with 30% limestone with vegetation grown on the top. (c) Before the remediation and (d) after the remediation. Plot numbers are as indicated. (e) Ernest Mine Watershed.

main source of geochemical input. The main concentrations and the pH values from the field observations at the Mather site (Table 2a) were used to initialize the corresponding values in the liquid within 0–61 cm and below 61 cm for plot 1 (i.e., 100% CR) and plot 2 (i.e., 90% CR + 10% BR), respectively, which correspond to the measurements made in June 2009. The total Fe concentration in the amended zone in plot 2 was much lower than that in plot 1 in Table 2a. This field observation is consistent with our simplified laboratory experiment, which was conducted in two glass columns with 73.7 cm in length: one column was filled with 100% CR and the other was filled with 30 cm of 90% CR + 10% BR on the top of 43 cm of 100% CR. Yellow ferric compounds were clearly observed to precipitate out at the surface of the remediated zone from the column with 90% CR + 10% BR while it was not observed in the column with 100% CR. The input data contain both the metals and nonmetals in the leachate.

The initial oxygen concentration profile for the six soil layers in the field, starting from the ground surface, is assumed to be: 0.25 kg/m^3, 0.20 kg/m^3, 0.15 kg/m^3, 0.02 kg/m^3, 0.01 kg/m^3 and 0.01 kg/m^3, respectively. The value of 0.25 kg/m^3 is based on the measurement of oxygen concentration at the ground surface. This study compares the model simulation with the field data for soil moisture and chemical concentrations.

There are numerous chemical elements associated with AMD, each having different impacts on the environment. For instance, the precipitates such as ferric iron hydroxides could obstruct biological activities through burial of substrata, clog gill surfaces and reduce light availability

Table 1
Porosity and saturated hydraulic conductivity for each plot at Mather site.

	Plot 1	Plot 2	Normal
Porosity	0.51	0.44	0.4
Ks ($m \cdot s^{-1}$)	0.00005	0. 00003	0. 00001

Table 2a
Initial condition and chemical compositions at Mather site. Initial solutions of chemical elements in total concentrations for 100% CR and 90% CR + 10% BR. Concentration units: ppm.

Materials	100% CR		90% CR + 10% BR	
Depth	0~61cm	below 61cm	0~61cm	below 61cm
pH	2.2	2.4	4.5	2.6
S as SO_4	5880	22800	1818	29394
Fe	1200	5500	5	9200
Ca	430	460	570	520
Na	200	365	280	1570
Mg	65	65	12	500
K	7.6	4.8	7.2	0.5
Si as SiO_2	177.9	186.4	60	212.7
P	15	52	0.5	190
Al	280	2000	1.6	1300
Cl	100	100	155	155
Mn	8.9	39	0.7	48

(DeNicola and Stapleton, 2002). The high levels of sulfate released during AMD could result in sulfide toxicity and damage the roots of aquatic plants (Lamers et al., 1998). Some Al compounds are toxic, such as aluminum oxide (Al_2O_3). Ca dissolution could result in high values of hardness of water and potentially increase the cost of water treatment. Based on the field measurements, concentrations of Fe (total), total S, total Al and total Ca in the AMD are relatively higher than the ones of the other elements. Thus, Fe, S, Al and Ca are the main elements to be discussed at the Mather site. The key mineral components found in CR include: Quartz, Pyrite, K-mica, Jarosite-K, Kaolinite, Calcite and Gypsum, which were all detected (Table 2b) by X-Ray Diffraction (XRD) in the CR samples of the study site.

The compositions of 90% CR + 10% BR, i.e., the amended zone in plot 2, mainly include Quartz, K-mica, Jarosite-K, Kaolinite, Dicalcium silicate, Sodalite, Calcite, Gehlenite, Gypsum, Hematite, Pyrite, Calcium aluminum sulfate, Calcium titanium oxide, Titanium dioxide and Gibbsite, which were detected in the mixing material sample and shown in Table 2c. Previous research has shown, based on the analyses of potential acidity production and acid neutralization, along with kinetic experiments, that a 10% BR/90%CR ratio will not potentially generate acid mine drainage and that this ratio is appropriate for long-term remediation (Plaza et al., 2017, 2018).

Similar to other geochemical modeling research (Gerke et al., 1998), Jarosite-K was not considered in this research. For plot 1, the concerned reactions are thus equations (R1) – (R3) and (R4) – (R8). The first three reactions are considered in PYROX and the remaining five reactions are included in the database of PHREEQC.

(R4) $CaCO_3 + 2\,H^+ \Leftrightarrow CO_2 + Ca^{2+} + H_2O$

(R5) $CaSO_4 \cdot 2H_2O \Leftrightarrow Ca^{2+} + SO_4^{2-} + 2\,H_2O$

(R6) $KAl_3Si_3O_{10}(OH)_2 + 10\,H^+ \Leftrightarrow K^+ + 3\,Al^{3+} + 3\,H_4SiO_4$

(R7) $Al_2Si_2O_5(OH)_4 + 6\,H^+ \Leftrightarrow H_2O + 2\,H_4SiO_4 + 2\,Al^{3+}$

(R8) $SiO_2 + 2H_2O \Leftrightarrow H_4SiO_4$

For plot 2, additional three components of Hematite (Fe_2O_3), Dicalcium silicate (Ca_2SiO_4) and Gehlenite ($Ca_2Al_2SiO_7$) were added into PHREEQC, which are represented by equations (R9) – (R11) below.

Table 2b
Initial condition and chemical compositions at Mather site. Solid compositions in 100% CR.

Composition	Percentage (%)
Quartz: SiO_2	55.62
K-mica: $KAl_2(AlSi_3O_{10}(OH)_2)$	24
Jarosite-K: $KFe_3(OH)_6(SO_4)_2$	9.9
Kaolinite: $Al_2O_32SiO_22H_2O$	8.26
Calcite: $CaCO_3$	1
Gypsum: $CaSO_4{\cdot}2H_2O$	0.92
Pyrite: FeS_2	0.3

(R9) $Fe_2O_3 + 6H^+ \Leftrightarrow 2Fe^{3+} + 3H_2O$

(R10) $Ca_2SiO_4 + 4H^+ \Leftrightarrow 2Ca^{2+} + H_4SiO_4$

(R11) $Ca_2Al_2SiO_7 + 10H^+ \Leftrightarrow H_4SiO_4 + 2Al^{3+} + 2Ca^{2+} + 3H_2O$

It is worth mentioning that the above reactions are not considered in the non-mine region and PHREEQC capabilities are turned off in this area.

Regarding the watershed case, Table 3 shows the initial solutions at the Ernest coal pile watershed. The initial solution of the regular soil (outside the coal pile), was adopted based on information from the literature (Agnieszka et al., 2012, Billett and Cresser, 1992, Klaminder et al., 2011, Lidman et al., 2017, Meers et al., 2006, Tack et al., 2002, Vandecasteele et al., 2002). The output location of the HTGCM model is at the MW-1 sampling site, whose data have also been included.

2.3. Experimental design

We designed an ensemble of three functional tests at the Mather site, which include the tests of soil moisture, soil temperature and chemical concentrations. We tested the HTGCM model at plot 1 and plot 2 to simulate hourly soil moisture and soil temperature from 4 May 2012 to 4 October 2012 using 3 × 3 m horizontal resolution. The observational data were used to calibrate and validate the model performance during this time period at plot 2, while plot 1 has no observed data. The field observation of chemical concentrations from 1 June 2009 to 27 June 2010 were used to compare with the HTGCM model's simulated concentrations since no chemical leaching data were collected in 2012. Here, we assume that the soil and heat parameters calibrated for 2012 do not have significant impacts on chemical concentrations over the period of 2009–2010. This assumption will be investigated once more datasets are collected in the future.

After the plot scale test, we run the HTGCM model at the Ernest Mine Watershed to test its capabilities at the watershed scale. In the "results

Table 2c
Initial condition and chemical compositions at Mather site. Solid compositions in 90% CR + 10% BR.

Composition	Percentage (%)
Quartz: SiO_2	50.358
K-mica: $KAl_2(AlSi_3O_{10}(OH)_2$	21.6
Jarosite-K: $KFe_3(OH)_6(SO_4)_2$	8.91
Kaolinite: $Al_2O_32SiO_22H_2O$	7.434
Dicalcium silicate: Ca_2SiO_4	5.7
Sodalite: $Na_8(Al_6Si_6O_{24})Cl_{12}$	1.2
Calcite: $CaCO_3$	1.2
Gehlenite: $Ca_2Al(AlSiO_7)$	1
Gypsum: $CaSO_4{\cdot}2H_2O$	0.828
Hematite: Fe_2O_3	0.8
Pyrite: FeS_2	0.27
Calcium aluminum sulfate: $Ca_6Al_2(SO_4)_3(OH)_{12}$	0.2
Calcium titanium oxide: $CaTiO_3$	0.2
Titanium dioxide: TiO_2	0.2
Gibbsite: Al(OH)3	0.1

Table 3
Initial solutions at Ernest Watershed.

Description	Amended Scenario	Non-amended Scenario	Outside Coal Pile
	Concentration (mg/L)	Concentration (mg/L)	Concentration (mg/L)
SO4	1000	3000	4.9
Fe	2	400	1.4
Ca	550	400	0.9
Na	280	200	2.2
Mg	100	65	100
K	7.2	8	0.3
Si	60	178	8.4
P	0.5	15	0.5
Al	1.5	200	1.7
Cl	155	100	0.001
Mn	2.0	40	0.007
Zn	0.0	2	0.009
Cr	0.004	0.6	0.002
Ni	0.01	2	0.003
Co	0.003	6	0.001
Cu	0.01	16	0.002
pH	6	4.5	5.5

and discussion" section, we will first show a near 2-year comparison between the model simulations and observations in the Ernest mine watershed before FBC ash addition. Then, a 2-year simulation with the same remediation strategy as the one used at the Mather site (i.e., 10% BR + 90 % CR amended layer) is presented. In addition, an extended simulation (10-year) of the non-amended scenario is presented and compared to the observed scenario with FBC ash addition.

Table 4
Comparison results of soil moisture and soil temperature between field measurement and model simulation at 61 cm in plot 2.

Simulated factors	RMSD	Sim. mean	Obs. mean	Abs. error	Relative error
Soil moisture (VWC)	0.02	0.19	0.20	0.001	0.45%
Soil temperature (°C)	1.54	20.60	19.54	1.06	5.44%

3. Results and discussion

3.1. Plot-based functional tests

3.1.1. Soil moisture

Fig. 4a and b show the simulated soil moisture at 61 cm in plots 1 and 2 at the Mather site. Only the field observation of soil moisture in plot 2 is compared to the model simulation since no measured soil moisture data were available (the strong acidity contained in the soil water of plot 1 destroyed the soil moisture sensors). Although there were a few spikes in the observed data in plot 2 which may be caused by the water pockets in the soil after the rain, the patterns of simulation and measurement are consistent. Table 4 provides the soil moisture comparison between the mean value of field observation (i.e., 0.20) and the mean value of model simulation (i.e., 0.19) in plot 2. The relative error between them is 0.45% and the root-mean-square deviation (RMSD) is 0.02. RMSD is the same as the RMSE (root-mean-square error) when they are used to compare difference between two series of values. These results suggest that the model performs well in simulating soil moisture comparing to the field measurements.

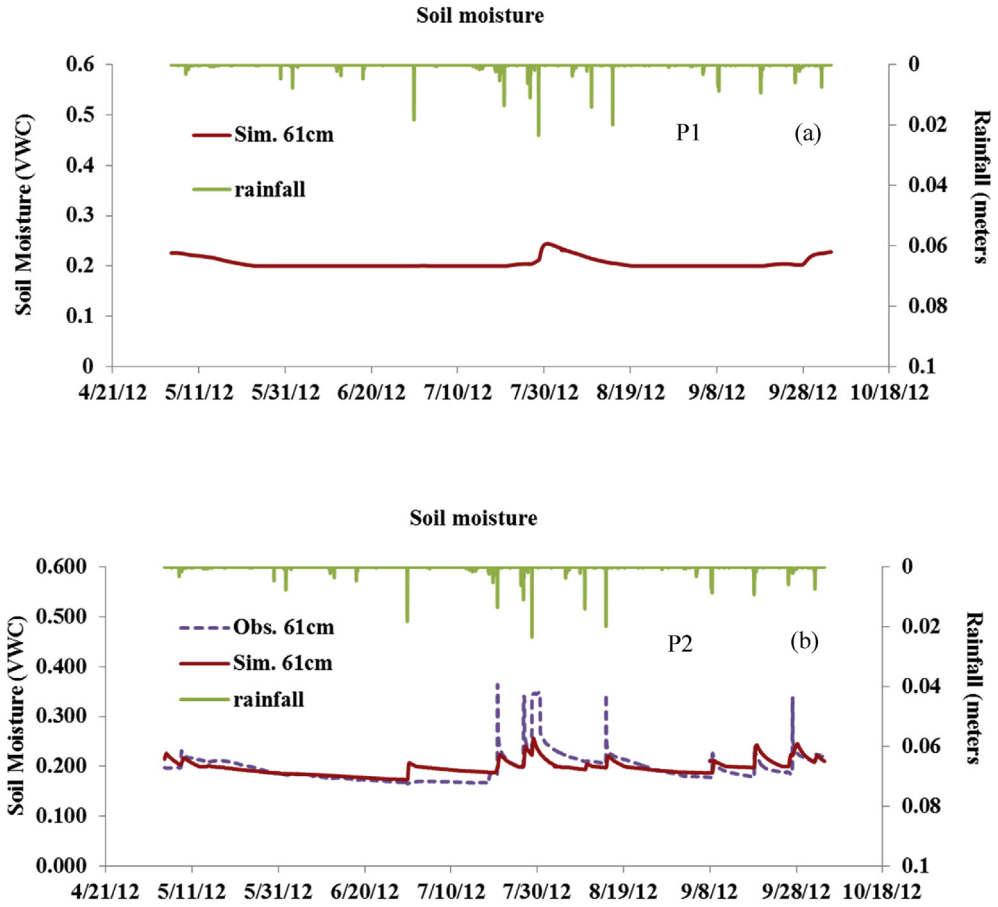

Fig. 4. Comparison between simulated and observed soil moisture at the 61 cm depth of the middle location along the hillslope of each plot from May 2012 to October 2012, where P1 (a) and P2 (b) represent plot1 and plot2, respectively. The detection limit of soil moisture is ± 0.03 m^3/m^3.

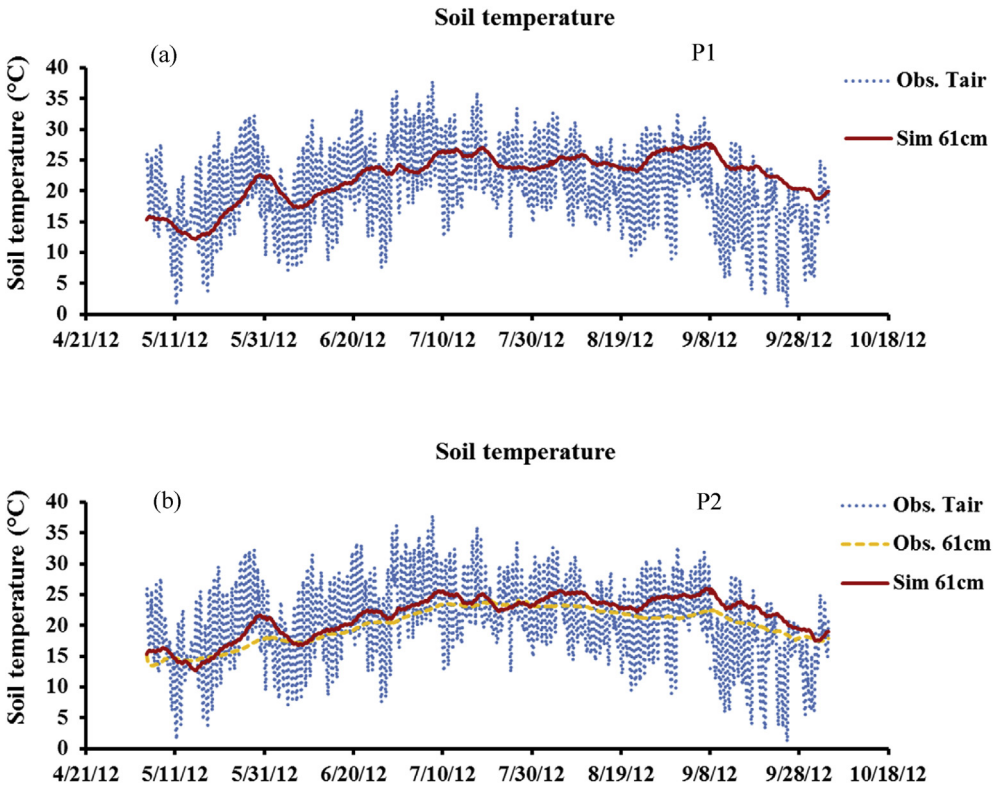

Fig. 5. Comparison between simulated and observed soil temperature at the 61 cm depth of the middle location along the hillslope of each plot from May 2012 to October 2012, where P1 (a) and P2 (b) represent plot1 and plot2, respectively. T_{air} represents air temperature. The detection limit of soil temperature is ±1 °C.

Table 5
Calibration results of heat parameters.

Heat parameter	Value
k_h, thermal conductivity (W/m K)	4.0
Cap_s, thermal capacity (J/m^3 K)	3.0e6
heatpro_A (J/m^3/day)	24.0
heatpro_B	0.008
heatpro_A_2 (J/m^3/day)	48.0
$decay_{chem}$	0.00001
$decay_{bio}$	0.00001

3.1.2. Soil temperature

Fig. 5a and b illustrate the simulated soil temperature at 61 cm in plots 1 and 2. Plot 1 did not have the field observation of soil temperature since the acidic water destroys the soil temperature sensors as well. The comparison between the model simulation and the field measurement in plot 2 is shown in Fig. 5b. A seasonal trend is indicated in the two plots, since a higher soil temperature was shown during summer time while a lower soil temperature was demonstrated in the periods of late spring and early fall. The modeled soil temperature compares well to the field observations. The soil temperature at 61 cm below the surface in plot 2 is much smoother than the air temperature as expected.

Table 4 also shows the soil temperature comparison between the mean value of field observation (i.e., 19.54 °C) and the mean value of model simulations (i.e., 20.6 °C) at 61 cm in plot 2. The relative error between them is 5.44% and the root-mean-square deviation (RMSD) is 1.54. Therefore, these results suggest that the model performs well in simulating soil temperature comparing to the field measurement.

The calibration results of heat parameters in plot 2 are shown in Table 5. Thermal conductivity was calibrated over the range of the mineral compositions (i.e., 0.3–7.7 Wm^{-1} K) (Gieré and Stille, 2004), which yielded a values of 4.0 Wm^{-1} K. Thermal capacity was calibrated over the range of 1.8×10^6–4.18×10^6 J m^{-3} K (Gieré and Stille, 2004) and the calibration result was 3.0e6 J m^{-3} K. The two decay parameters (i.e., $decay_{chem}$ and $decay_{bio}$) were calibrated with a 50 years' half-life time period. Values of the parameters of heatpro_A, heatpro_B, heatpro_A_2 and n were also obtained from model calibration. Due to the lack of field measurements for these four parameters and the limited information in the technical literature, we do not have the ranges for these parameters. All of the parameters were calibrated manually. For plot 1, no observed data are available to calibrate the relevant model parameters and thus the corresponding values obtained from plot 2 are used to conduct the simulations.

3.1.3. Chemical concentrations: pH, sulfate, metals/nonmetals

Fig. 6 shows the simulations of SO_4, Fe (total), total Ca (Ca^{2+} in all Ca solutions), total Al (Al^{3+} in all Al solutions) and pH in soil water at 61 cm deep in plot 1 and plot 2. Relative errors between field observations and model simulations are 2% and 0.13% for SO_4 and Fe (total), respectively for plot 1. In plot 2, the simulated SO_4 and Fe (total) captured the patterns of field observations as well, although the relative errors are 11% and over 100% for SO_4 and Fe (total), respectively. The much higher relative errors in plot 2 are due to the much lower concentrations in plot 2 than those in plot 1 except for the total calcium which might be caused by the dissolution of Ca carbonates, such as calcite (CaCO3), due to the alkaline additive, thus releasing Ca (Plaza et al., 2017). Usually, calcite is identified with acidic neutralization, enabling various metal removal mechanisms (Sun et al., 2013). However, high dissolution rates of Ca minerals could also occur in active mine tailings (e.g., CR). As expected, the alkaline materials added to plot 2 increased the pH value allowing for more SO_4^{2-}, Fe^{3+} and Al^{3+} to precipitate into the solids. For the total calcium concentrations, they were similar in both plots based on the field measurements. The lower Fe concentration shown in plot 2 is due to that ferric iron can easily precipitate from plot 2 with the addition of alkaline materials, which has been confirmed by the laboratory experiments.

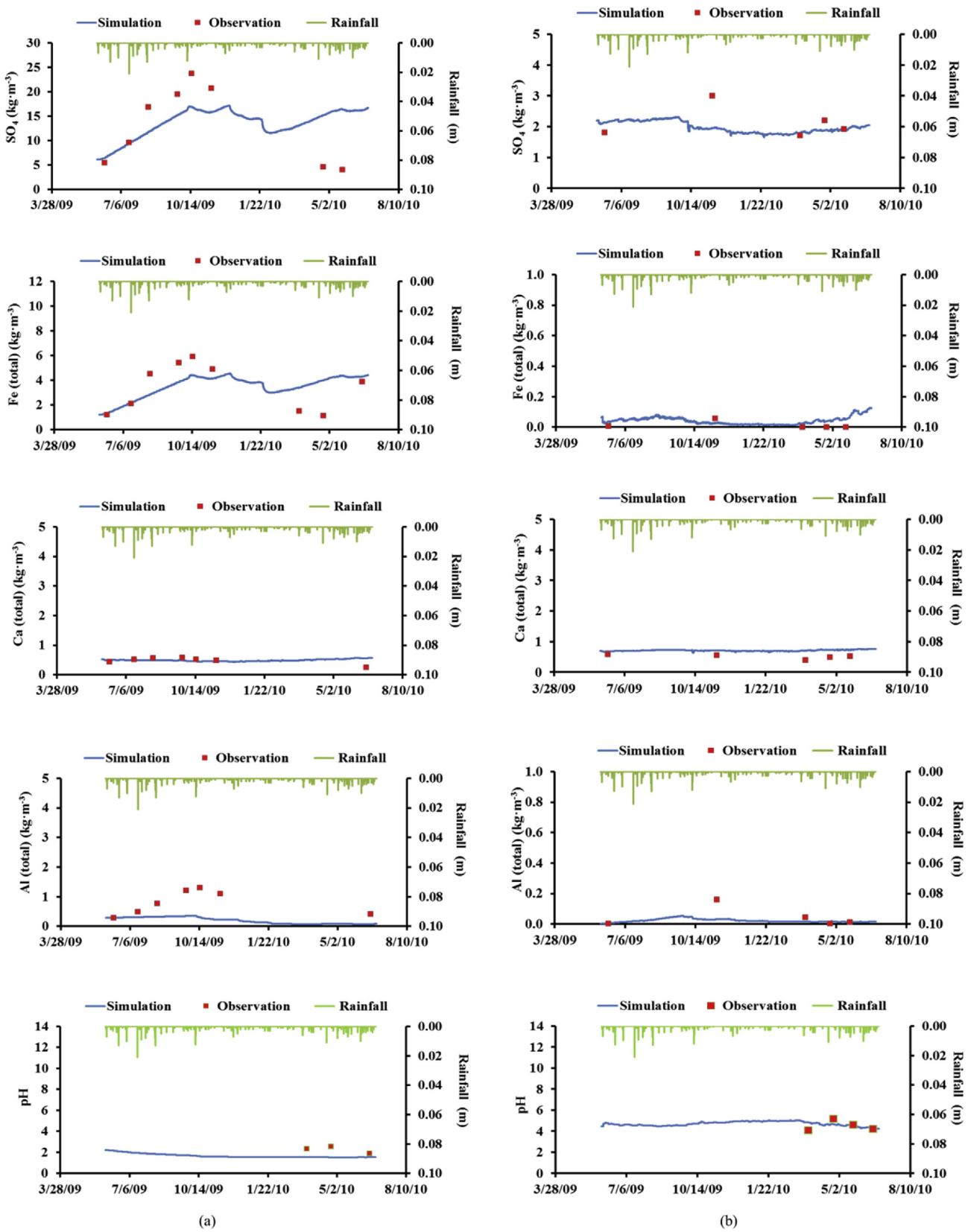

Fig. 6. (a) The simulations of SO_4, Fe (total), Ca (total), Al (total) and pH at the depth of 61 cm from June 2009 to June 2010 in plot 1 (left). (b) The simulations of SO_4, Fe (total), Ca (total), Al (total) and pH at the depth of 61 cm from June 2009 to June 2010 in plot 2 (right).

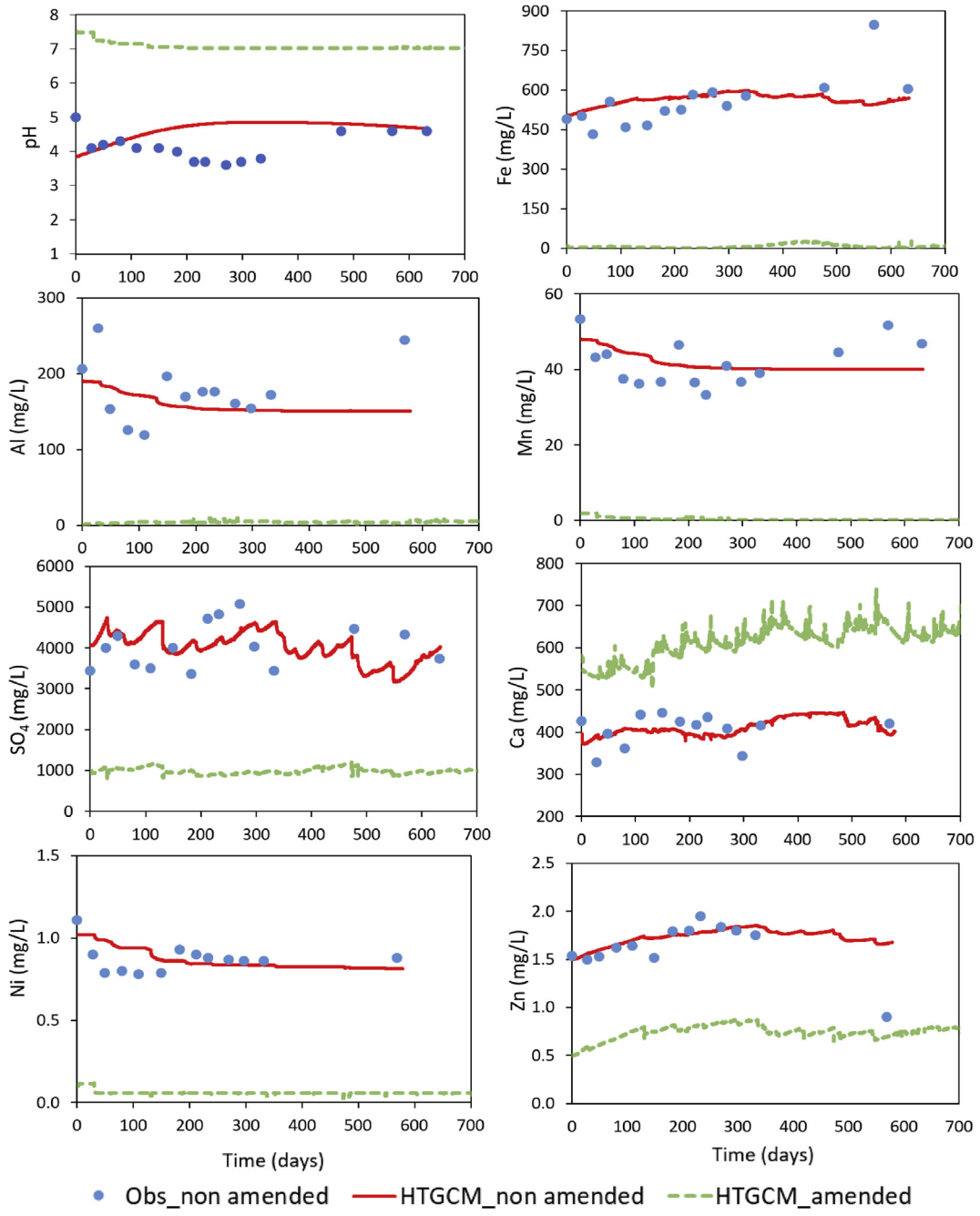

Fig. 7. Ernest Mine Watershed HTGCM 2-yr simulations for amended and non-amended conditions. The observed data is for the non-amended scenario. Field observation shown in the plots were measured from November 1994 to August 1996.

3.2. *Watershed modeling test*

3.2.1. *Implementation of the HTGCM model in the Ernest coal pile watershed*

Fig. 7 presents simulation results (approximately 2 years) of the HTGCM model applied to the Ernest mine watershed at the watershed scale. Simulation results considering the same remediation design as the one tested in Mather (10% BR + 90 % CR amended layer) are also included in Fig. 7 for comparison. Fig. 8 presents an extended simulation (10-year) of the non-amended scenario. The field observations before (i.e., non-amended) and after the addition of FBC ash (i.e., amended) are also included in Fig. 8. The water quality data were from the MW-1 sampling site after the addition of FBC ash (i.e., amended).

As previously mentioned, there is an evidence (Pennsylvania Minefill Study, 2007) pointing to the fact that the addition of FBC ash not only did not improve the water quality conditions, but caused a water quality degradation process. In June, 2002, the Pennsylvania Department of Environmental Protection (PADEP) issued a report on the Ernest site responding to public concerns about the water quality degradation from this operation. The last recorded water quality data available for this site are from November 2004. In the model results, all the available data are presented. However, only the data before the FBC ash placement when the site was an unaltered coal refuse pile are utilized for the purposes of the model assessment.

3.2.2. *Watershed modeling discussion*

From Fig. 7, it can be seen that the HTGCM model properly captures the behavior of the system for the non-amended scenario for the Ernest

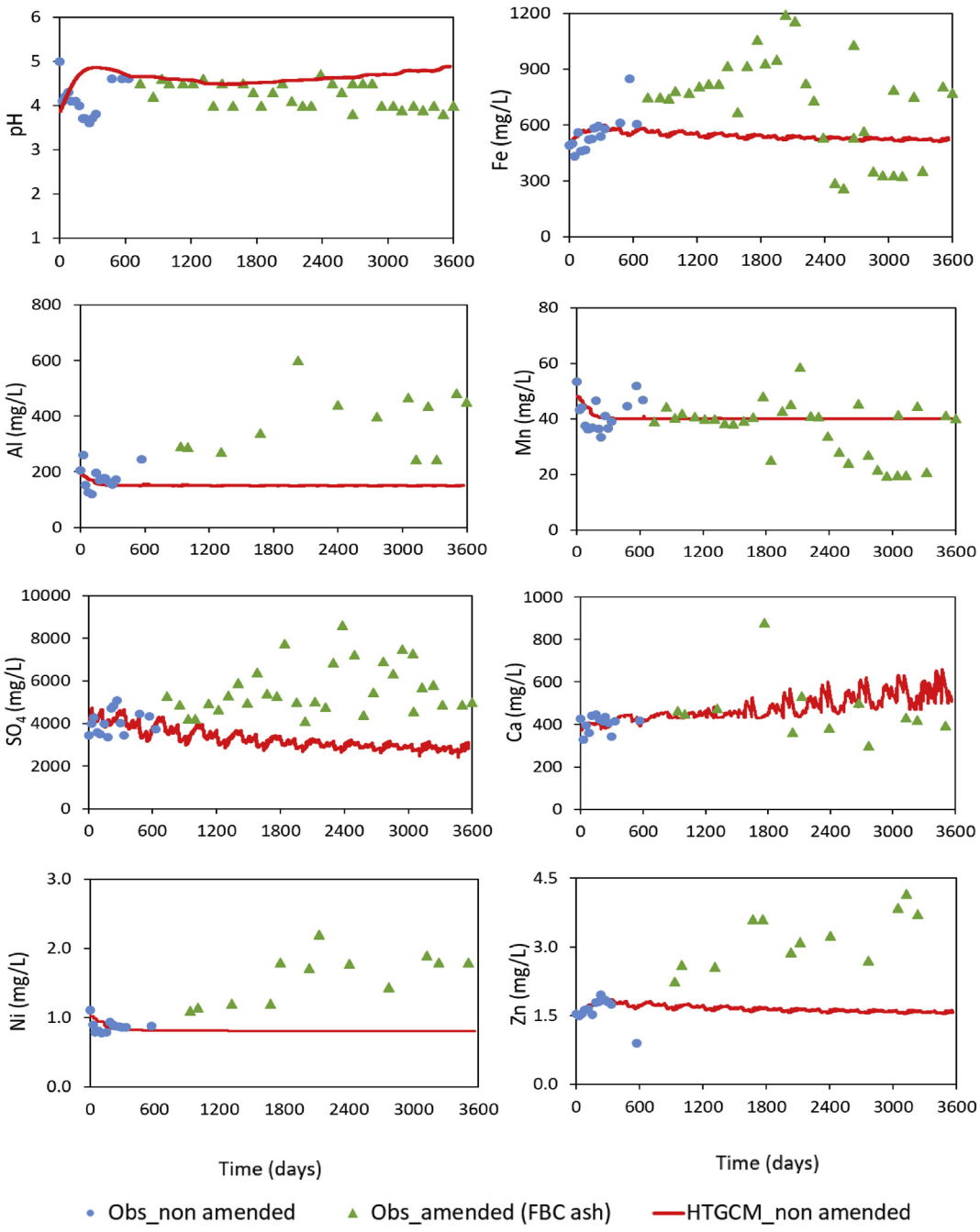

Fig. 8. Ernest Mine Watershed HTGCM 10-yr simulations (1994–2004) and observed data before and after the addition of FBC ash. Field observation shown in the plots were measured from November 1994 to August 1996 (i.e., before FBC ash addition) and from November 1996 to September 2004 (i.e., after FBC ash addition).

mine site. Moreover, it is probable that the water quality measured at MW-1 is influenced by a dilution effect caused by the contribution of surface and subsurface drainage from the non-mine region (9.51 km^2). This is inferred by the relatively low chemical concentrations and higher pH for the non-amended scenario at MW-1 when compared to those field observed data from the coal refuse site at Mather. For instance, at Mather (non-amended plot 1 at 91 cm) the pH, SO_4, Fe, Ni and Zn concentrations range approximately (from June 2009 to June 2010) from 3 – 2, 9000–7000 mg/L, 9000–5000 mg/L, 20–5 mg/L and 40–20 mg/L, respectively, while at Ernest (non-amended pile in MW-1 at 150 cm depth), the pH, SO_4, Fe, Ni and Zn concentrations range approximately (from November 1994 to August 1996) from 4 – 4.5, 5000–3000 mg/L, 600–500 mg/L, 1–0.8 mg/L and 2–1.5 mg/L, respectively, considering the same period of time in both cases. This fact emphasizes the importance and necessity of including the entire watershed in the model simulation study and the hydrogeochemical interactions between the mine and non-mine areas in the model. In other words, it is important to assess the environmental impacts of the coal refuses at multiple locations, both inside and outside the mine site, within a watershed.

The amended scenario simulation in Fig. 7 should be taken only as a reference to illustrate how the conditions in Ernest would have been changed if a similar remediation design as the one applied to the experimental plots in Mather had been applied to Ernest as well (i.e., neutral pH and high immobilization of SO_4 and toxic metals). It is not necessary to extend this simulation, as there are no field observation to compare with.

Regarding the extended simulation period (Fig. 8), one can see that some chemicals, such as SO_4, Fe, Al, Ni and Zn, reached higher

concentrations after the remediation was applied at the site. This might imply a lack of characterization study of the FBC ash as a remediation material, because this material apparently generated the mobilization of higher amounts of some chemicals compared to the case of the non-amended conditions. This demonstrates the importance of developing/using an appropriate model (e.g., HTGCM) to conduct a long-term model simulation (e.g., HTGCM_non amended) and of carrying out an extensive hydrogeochemical analysis of the remediation material (e.g., FBC ash) in exploring potential remediation strategies. On the other hand, other chemicals such as pH and Ca remained stable while Mn was observed to have a slightly oscillatory behavior. It is worth mentioning that the model calibration was solely based on the field observation before the addition of the FBC ash and the long-term simulation is intent to replicate the conditions that would have experienced at the site if no remediation had ever been made. Non-amended conditions (simulated) happened to be, in most cases, less critical than the observed conditions with the addition of an AMD remediation agent.

4. Conclusions

A new hydro-thermal-geochemical model (HTGCM), which incorporates the hydrologic and kinetic processes of pyrite oxidation, was developed. Not only can this model represent the dynamics of the water and energy cycles (e.g., soil moisture and soil temperature) with physically-based hydrological processes, but can also describe the chemical dynamics of pyrite oxidation: the behavior of SO_4, Fe (total), Ca, Al, pH and the other constituents within a coal refuse pile. The high-resolution nature of the HTGCM model makes it possible to capture the characteristics related to the hydro-thermal-geochemical processes at a small scale (e.g., plot scale) and also, to represent the integrated impacts of these processes at a larger scale (e.g., watershed scale) through an effective routing network in which both the water and chemical concentrations are accounted for.

At a plot scale, the modeling results of HTGCM on soil moisture, soil temperature and chemical concentrations are compared with the field observations collected at multiple locations along the hillslope within the coal refuse pile at the Mather site. The model simulations show promising results for soil moisture and soil temperature, and encouraging results for chemical concentrations at the Mather site, thus revealing the impact of the BR treatment on reducing the chemical concentrations and neutralizing acidity.

At a watershed scale, HTGCM is able to reproduce the chemical concentrations in the non-amended scenario very well compared to the observations, although no comparisons are made between the model simulated results and the amended observations due to the lack of data. These modeling results (i.e., at the Mather and Ernest sites) demonstrate that HTGCM is applicable to spatial scales ranging from a point to a watershed.

In summary, the main findings of this study include: (1) HTGCM is capable of successfully reproducing the reactive transport processes for the non-amended and amended scenarios at a mine-impacted watershed, since the modeling results (e.g., soil moisture, soil temperature and chemical concentrations) are consistent with the observations; and (2) HTGCM allows the assessment of the AMD generation and remediation impacts, inside and outside the waste coal pile.

The beneficial use of two waste products presents a unique approach for the remediation of the AMD legacy problem as exemplified at the coal-refuse pile at Mather, PA. This study presents the HTGCM model as a useful modeling tool to investigate impacts of AMD/treated region on its environment at different spatial scales.

Declaration

Author contribution statement

Yi Xu, Fernando Plaza: Conceived and designed the experiments; Performed the experiments; Analyzed and interpreted the data; Wrote the paper.

Xu Liang: Conceived and designed the experiments; Analyzed and interpreted the data; Contributed reagents, materials, analysis tools or data; Wrote the paper.

Tyler W. Davis: Performed the experiments; Analyzed and interpreted the data.

Judodine Nichols, Jaw K. Fu, Peter Koranchie-Boah: Analyzed and interpreted the data; Contributed reagents, materials, analysis tools or data.

Funding statement

This work was partially supported by the National Science Foundation under CBET-1236403 and by Alcoa to the University of Pittsburgh. Xu Liang also acknowledges the support from the William Kepler Whiteford Professorship from the University of Pittsburgh.

Competing interest statement

The authors declare no conflict of interest.

Additional information

No additional information is available for this paper.

Acknowledgements

The authors would like to thank Jason D. Monnell for his help and for providing necessary laboratory equipment at the beginning stage of this project. We thank James M Segneff for his help on computing related issues and the Center for Research Computing for providing the computing resources at the University of Pittsburgh. We also thank Vicky Deng and Yipei Wen for their efforts in performing some of the laboratory tests. The data used are listed in the references and tables. The KPACLARK3 and KPAINDIA4 Weather Underground stations are acknowledged for the weather data.

References

Agnieszka, J., Barbara, G., 2012. Chromium, nickel and vanadium mobility in soils derived from fluvioglacial sands. J. Hazardous Mater. 237–238, 315–322.

Allison, J.D., Brown, D.S., Novo-Gradac, K.J., 1991. MINTEQA2/PRODEFA2, a Geochemical Assessment Model for Environmental Systems :Version 3.0 User's Manual*Rep*. Environmental Research Laboratory, Office of Research and Development, U. S. Environmental Protection Agency, Athens, Georgia,U.S.A.

Brown, P., Crawford, J., Irannejad, P., Miskelly, P., Noël, M., Pantelis, G., Plotnikoff, W., Sinclair, D., Stepanyants, Y., 2001. SULFIDOX: Version 1.1. A Tool for Modelling the Temporal and Spatial Behaviour of Heaps Containing Sulfidic minerals*Rep.*, ANSTO Technical Report, ANSTO/ED/TN01-03.

Charlton, S.R., Parkhurst, D.L., 2011. Modules based on the geochemical model PHREEQC for use in scripting and programming languages. Comput. Geosci. UK 37 (10), 1653–1663.

Charlton, S.R., Macklin, C.L., Parkhurst, D.L., 1997. PHREEQCI—A Graphical User Interface for the Geochemical Computer Program PHREEQC*Rep*. U.S. GEOLOGICAL SURVEY, Lakewood, CO.

Chen, L., Young, M.H., 2006. Green-Ampt infiltration model for sloping surfaces. Water Resour. Res. 42 (7), W07420.

da Silva, J.C., do Amaral Vargas, E., Sracek, O., 2009. Modeling multiphase reactive transport in a waste rock pile with convective oxygen supply. Vadose Zone J. 8 (4), 1038–1050.

Davis, G.B., Ritchie, A.I.M., 1986. A model of oxidation in pyritic mine wastes .1. equations and approximate solution. Appl. Math. Model. 10 (5), 314–322.

DeNicola, D.M., Stapleton, M.G., 2002. Impact of acid mine drainage on benthic communities in streams: the relative roles of substratum vs. aqueous effects. Environ. Pollut. 119 (3), 303–315.

Doten, C.O., Bowling, L.C., Lanini, J.S., Maurer, E.P., Lettenmaier, D.P., 2006. A spatially distributed model for the dynamic prediction of sediment erosion and transport in mountainous forested watersheds. Water Resour. Res. 42 (4).

Elberling, B., Nicholson, R.V., David, D.J., 1993. Field-evaluation of sulfide oxidation rates. Nord. Hydrol 24 (5), 323–338.

Gerke, H.H., Molson, J.W., Frind, E.O., 1998. Modelling the effect of chemical heterogeneity on acidification and solute leaching in overburden mine spoils. J. Hydrol. 209 (1-4), 166–185.

Gieré, R., Stille, P., 2004. Energy, waste and the environment: a geochemical perspective. Geol. Soc. Am.

Hollesen, J., Elberling, B., Jansson, P.E., 2011. Modelling temperature-dependent heat production over decades in High Arctic coal waste rock piles. Cold Reg. Sci. Technol. 65 (2011), 258–268.

Jacques, D., Šimůnek, J., Mallants, D., van Genuchten, M.T., 2006. Operator-splitting errors in coupled reactive transport codes for transient variably saturated flow and contaminant transport in layered soil profiles. J. Contam. Hydrol. 88 (3), 197–218.

Johnson, D.B., 2003. Chemical and microbiological characteristics of mineral spoils and drainage waters at abandoned coal and metal mines. Water Air Soil Pollut.: Focus 3 (1), 47–66.

Johnson, D.B., Hallberg, K.B., 2005. Acid mine drainage remediation options: a review. Sci. Total Environ. 338 (1-2), 3–14.

Kameia, G., Ohmoto, H., 2000. The kinetics of reactions between pyrite and O-2-bearing water revealed from in situ monitoring of DO, Eh and pH in a closed system. Geochem. Cosmochim. Acta 64 (15), 2585–2601.

Klaminder, J., Grip, H., Morth, C.-M., Laudon, H., 2011. Carbon mineralization and pyrite oxidation in groundwater: importance for silicate weathering in boreal forest soils and stream base-flow chemistry. Appl. Geochem. 26, 319–324.

Lamers, L.P., Tomassen, H.B., Roelofs, J.G., 1998. Sulfate-induced eutrophication and phytotoxicity in freshwater wetlands. Environ. Sci. Technol. 32 (2), 199–205.

Lawrence, D., et al., 2019. Technical Description of Version 5.0 of the Community Land Model (CLM), *National Center for Atmospheric Research P. O. Box 3000, Boulder, Colorado 80307-300*.

Lefebvre, R., 1994. Characterization and Numerical Modeling of Acid Mine Drainage in Waste Rock dump.(In French.), Ph.D. Thesis. Univ. Laval, Quebec, Canada.

Leung, L., Wigmosta, M., Ghan, S., Epstein, D., Vail, L., 1996. Application of a subgrid orographic precipitation/surface hydrology scheme to a mountain watershed. J. Geophys. Res.: Atmosphere 101 (D8), 12803–12817.

Leung, L.R., Wigmosta, M.S., 1999. Potential climate change impacts ON mountain watersheds IN the pacific NORTHWEST1. J. Am. Water Resour. Assoc. 35 (6), 1463–1471.

Liang, X., Lettenmaier, D.P., Wood, E.F., Burges, S.J., 1994. A simple hydrologically based model of land-surface water and energy fluxes for general-circulation models. J. Geophys. Res. Atmos. 99 (D7), 14415–14428.

Lidman, F., Boily, Å., Laudon, H., Köhler, S.J., 2017. From soil water to surface water – how the riparian zone controls element transport from a boreal forest to a stream. Biogeosciences 14, 3001–3014.

Mayer, K.U., Frind, E.O., Blowes, D.W., 2002. Multicomponent reactive transport modeling in variably saturated porous media using a generalized formulation for kinetically controlled reactions. Water Resour. Res. 38 (9), 1174.

Meers, E., Du Laing, G., Unamuno, V.G., Lesage, E., Tack, F.M.G., Verloo, M.G., 2006. water extractability of trace metals from soils: some pitfalls. Water Air Soil Pollut. 176, 21.

Mitchell, K., 2001. The community Noah land-surface model (LSM), *User, s Guide*. Publ. Release Version 2 (7), 1.

Molson, J., Fala, O., Aubertin, M., Bussière, B., 2005. Numerical simulations of pyrite oxidation and acid mine drainage in unsaturated waste rock piles. J. Contam. Hydrol. 78 (4), 343–371.

Pantelis, G., Ritchie, A.I.M., Stepanyants, Y.A., 2002. A conceptual model for the description of oxidation and transport processes in sulphidic waste rock dumps. Appl. Math. Model. 26 (7), 751–770.

Parkhurst, D., Appelo, C., 2013. Description of input and examples for PHREEQC version 3—a computer program for speciation, batch-reaction, one-dimensional transport, and inverse geochemical calculations. Modeling Tech. 6.

Parkhurst, D.L., 1995. User's guide to PHREEQC: a computer program for speciation,reaction-path, advective transport, and inverse geochemical calculations. Water Res. Investig. Rep. 95 (4227). USGS, Lakewood, Colorado.

Parkhurst, D.L., Appelo, C.A.J., 1999. User's guide to PHREEQC (version 2)–A computer program for speciation, batch-reaction, one-dimensional transport, and inverse geochemical calculations:U.S. Geological Survey. Water Res. Investig. Rep. 99 (4259), 4312. Denver, Colorado.

Parkhurst, D.L., Th orstenson, D.C., Plummer, L.N., 1980. PHREEQE: a computer program for geochemical calculations. US Geol. Surv. Water Resour. Invest. 80–96. USGS, Lakewood, Colorado.

Pennsylvania Minefill Study, 2007. Impacts of Water Quality from Placement of Coal Combustion Waste in Pennsylvania Coal Mines. Clean Air Task Force.

Philip, J.R., 1991. Hillslope infiltration:planar slopes. Water Resour. Res. 27 (1), 109–117.

Plaza, F., Wen, Y., Liang, X., 2018. Acid rock drainage passive remediation using alkaline clay: hydro-geochemical study and impacts of vegetation and sand on remediation. Sci. Total Environ. 637-638, 1262–1278.

Plaza, F., Wen, Y., Perone, H., Xu, Y., Liang, X., 2017. Acid rock drainage passive remediation: potential use of alkaline clay, optimal mixing ratio and long-term impacts. Sci. Total Environ. 576, 572–585.

Pruess, K., 1991. TOUGH2: A General-Purpose Numerical Simulator for Multiphase Fluid and Heat Transfer, LBL-29400. Lawrence Berkeley Laboratory, Berkeley, CA.

Silva, J.C., 2004. Modeling and Numerical Simulation of Multiphase Transport in Porous media with Thermo-Chemical Interactions (In Portuguese), Ph.D. Thesis. Catholic Univ. of Rio de Janeiro, Brazil.

Šimůnek, J., Huang, K., Van Genuchten, M.T., 1998. The HYDRUS Code for Simulating the One-Dimensional Movement of Water, Heat, and Multiple Solutes in Variably-Saturated media,Version 6.0, Research Report No. 144. U.S. Salinity Laboratory, USDA, ARS,*Rep.*, Riverside, California.

Šimůnek, J., Sejna, M., van Genuchten, M.T., 1999. The Hydrus-2D Software Package for Simulating Two-Dimensional Movement of Water, Heat, and Multiple Solutes in Variably Saturated media. Version 2.0/GWMC-TPS - 53*Rep.*, p. 251.

Šimůnek, J., van Genuchten, M.T., Sejna, M., 2008. Development and applications of the HYDRUS and STANMOD software packages and related codes. Vadose Zone J. 7 (2), 587–600.

Stange, C.F., 2007. A novel approach to combine response functions in ecological process modelling. Ecol. Model. 204, 547–552.

Stumm, W., Morgan, J.J., 1981. Aquatic Chemistry:An Introduction Emphasizing Chemical Equilibria in Natural Waters. John Wiley & Sons, New York.

Sun, J., Tang, C., Wu, P., Strosnider, W.H.J., Han, Z., 2013. Hydrogeochemical characteristics of streams with and without acid mine drainage impacts: a paired catchment study in karst geology, SW China. J. Hydrol. 504, 115–124.

Tack, F.M.G., Dezillie, N., Verloo, M.G., 2002. Metal concentrations in soil paste extracts as affected by extraction ratio. Sci. World J. 2, 966–971.

Vandecasteele, B., De Vos, B., Tack, F.M.G., 2002. Heavy metal contents in surface soils along the upper scheldt river (Belgium) affected by historical upland disposal of dredged materials. Sci. Total Environ. 290, 1–14.

Walter, A.L., Frind, E.O., Blowes, D.W., Ptacek, C.J., Molson, J.W., 1994. Modeling of multicomponent reactive transport in groundwater .1. Model development and evaluation. Water Resour. Res. 30 (11), 3137–3148.

Westrick, K.J., Storck, P., Mass, C.F., 2002. Description and evaluation of a hydrometeorological forecast system for mountainous watersheds. Weather Forecast. 17 (2), 250–262.

Whitaker, A., Alila, Y., Beckers, J., Toews, D., 2002. Evaluating peak flow sensitivity to clear-cutting in different elevation bands of a snowmelt-dominated mountainous catchment. Water Resour. Res. 38 (9).

Wigmosta, M.S., Lettenmaier, D.P., 1999. A comparison of simplified methods for routing topographically driven subsurface flow. Water Resour. Res. 35 (1), 255–264.

Wigmosta, M.S., Vail, L.W., Lettenmaier, D.P., 1994. A distributed hydrology-vegetation model for complex terrain. Water Resour. Res. 30 (6), 1665–1679.

Williamson, M.A., Rimstidt, J.D., 1994. The kinetics and electrochemical rate-determining step of aqueous pyrite oxidation. Geochem. Cosmochim. Acta 58 (24), 5443–5454.

Wunderly, M.D., Blowes, D.W., Frind, E.O., Ptacek, C.J., 1996. Sulfide mineral oxidation and subsequent reactive transport of oxidation products in mine tailings impoundments: a numerical model. Water Resour. Res. 32 (10), 3173–3187.